

## Chapter 4

# Photocatalytic Production of Hydrogen on Ni/NiO/ $\text{KNbO}_3$ /CdS Nanocomposites using Visible Light

Sections reprinted with permission from Choi, J.; Ryu, S.Y.; Balcerski, W.; Lee, T.K.; Hoffmann, M. R. *Journal of Materials Chemistry* **2008**, *18*, 2371.  
© 2008 The Royal Society of Chemistry

## Abstract

The photocatalytic production of H<sub>2</sub> from water splitting was demonstrated on Ni/NiO/KNbO<sub>3</sub>/CdS nanocomposites using visible light irradiation at wavelengths > 400 nm in presence of isopropanol. The inherent photocatalytic activity of bulk-phase CdS was enhanced by combining Q-sized CdS with KNbO<sub>3</sub> and Ni deposited on KNbO<sub>3</sub>. Enhanced activity is most likely due to effective charge separation of photogenerated electrons and holes in CdS that is achieved by electron injection into the conduction band of KNbO<sub>3</sub> and the reduced states of niobium (e.g., Nb(IV) and Nb(III)) are shown to contribute to enhanced reactivity in the KNbO<sub>3</sub> composites by mediating effective electron transfer to bound protons. We also observed that the efficient attachment of Q-size CdS and the deposition of nickel on the KNbO<sub>3</sub> surface increases H<sub>2</sub> production rates. Other factors that influence the rate of H<sub>2</sub> production including the nature of the electron donors and the solution pH were also determined. The Ni/NiO/KNbO<sub>3</sub>/CdS nanocomposite system appears to be a promising candidate for possible practical applications including the production of H<sub>2</sub> under visible light.

## Introduction

Hydrogen ( $H_2$ ) production from water splitting using semiconductor photocatalysts has attracted considerable interest since the pioneering work of Fujishima and Honda,<sup>1</sup> who discovered that water can be photo-electrochemically decomposed into hydrogen and oxygen using a semiconductor ( $TiO_2$ ) electrode under UV irradiation. A large number of metal oxides and sulfides (e.g.  $TiO_2$ ,<sup>1-3</sup>  $WO_3$ ,<sup>4-6</sup>  $SrTiO_3$ ,<sup>7,8</sup>  $ZnO$ ,<sup>9-11</sup>  $CdS$ ,<sup>12-17</sup>  $ZnS$ ,<sup>13,16,18,19</sup> niobates,<sup>20-24</sup> and tantalates<sup>25-28</sup>) have been examined as photocatalysts for hydrogen production from splitting water. However, the majority of the simple and mixed-metal oxides photocatalysts are primarily active for  $H_2$  production under UV irradiation ( $\lambda < 385$  nm or  $E_{bg} \geq 3.0$  eV) present in only a small portion of solar light. More recently, there is a focused effort on the development of photocatalysts that are capable of using visible light ( $\lambda = 400\text{--}700$  nm) for the photocatalytic production of  $H_2$  including transition metal doping (e.g., platinum,<sup>29</sup> chromium,<sup>30</sup> and vanadium<sup>31</sup>) and nonmetallic element doping (e.g., nitrogen,<sup>32-35</sup> sulfur,<sup>36,37</sup> and carbon<sup>35,38</sup>).

$CdS$ , n-type semiconductor with  $E_g = 2.4$  eV, has been shown to have photocatalytic activity for  $H_2$  production under visible light irradiation, although, sacrificial electron donors such as  $C_2H_5OH$ ,<sup>39</sup>  $HS^-$ ,<sup>40,41</sup> or  $SO_3^{2-}$ <sup>19</sup> are used to obtain measurable rates of  $H_2$  production and to avoid the photocorrosion of  $CdS$  in the presence of  $O_2$ . On the other hand, the electronic levels and photoactivity of  $CdS$  can be tuned by changing or controlling particle size without changing the chemical composition. For example in the case of nanoparticulate  $ZnO$ , Hoffmann and co-workers<sup>9,42</sup> reported a tenfold increase in photoefficiency for the photocatalytic production of hydrogen peroxide with a decrease in particle size from 40 to 23 nm. In another example, Hoffman et al.<sup>43</sup> found an increase

in quantum efficiency for photo-polymerization of methylmethacrylate with a corresponding decrease in particle size using Q-size CdS.

In order to enhance the photocatalytic activity of CdS, efforts have been made to combine CdS with other semiconductors having different band energies (e.g., TiO<sub>2</sub>,<sup>44-47</sup> ZnS,<sup>13,48,49</sup> K<sub>4</sub>Nb<sub>6</sub>O<sub>17</sub>,<sup>50</sup> or K<sub>2</sub>Ti<sub>4</sub>O<sub>9</sub><sup>51,52</sup>) since the coupling of two semiconductor particles with different energy levels is useful to achieve effective charge separation. For example in a colloidal TiO<sub>2</sub>/CdS composite system, the electrons photogenerated from CdS band gap excitation can be transferred to the conduction band (CB) of TiO<sub>2</sub> particles, while the holes remain in the CdS particle. It is also observed that this charge separation in a colloidal composite system can accelerate the degradation of azo-dye<sup>44</sup> and increase H<sub>2</sub> production in aqueous H<sub>2</sub>S solution.<sup>46</sup>

In this study, we synthesized nanocomposites of potassium niobate (KNbO<sub>3</sub>) and CdS by solid-state reactions and investigated their properties and photoactivity for H<sub>2</sub> production under visible light irradiation ( $\lambda > 400$  nm) in presence of isopropanol as an electron donor. KNbO<sub>3</sub> is used in optical waveguides, in nonlinear optical devices (e.g., frequency doubling and wavelength mixing), in piezoelectric devices (e.g., tunable frequency ultrasound transducers), in holographic image storage, and as a wide-band gap photocatalyst ( $\Delta E_g = 3.4$  eV) because of its unusual chemical and physical properties. KNbO<sub>3</sub>/CdS nanocomposites are characterized by XRD, SEM, TEM, UV-vis reflectance spectra and show better visible-light photoactivity for H<sub>2</sub> production than other composites (e.g., TiO<sub>2</sub> or K<sub>4</sub>Nb<sub>6</sub>O<sub>17</sub>). Moreover, the efficiency of H<sub>2</sub> production is significantly enhanced by loading Ni on KNbO<sub>3</sub>.

## Experimental

### Sample Preparation

Stoichiometric KNbO<sub>3</sub> was synthesized from Nb<sub>2</sub>O<sub>5</sub> (Aldrich) and K<sub>2</sub>CO<sub>3</sub> (Aldrich) in a standard solid-state reaction. K<sub>2</sub>CO<sub>3</sub> and Nb<sub>2</sub>O<sub>5</sub> were mixed together in a mortar at 1:1 mole ratio and the powdered mixture was pressed into a pellet at 27.6 Mpa and then heated at 650~925 °C for 10 hours with a heating and cooling temperature ramp of ±200 °C/h. With slight variations of the K:Nb mole ratio of 1:1.1 and a heating temperature at 1025 °C, a mixture of KNbO<sub>3</sub> and K<sub>4</sub>Nb<sub>6</sub>O<sub>17</sub> was obtained. Synthesis of K<sub>4</sub>Nb<sub>6</sub>O<sub>17</sub> was carried out for comparison using K<sub>2</sub>CO<sub>3</sub> and Nb<sub>2</sub>O<sub>5</sub> in the K:Nb mole ratio of 1:1.5 and calcination at 1150 °C for 10 hours. The crystal structures were confirmed by X-ray diffraction (XRD) at room temperature.

KNbO<sub>3</sub>/CdS composite samples were prepared by stirring KNbO<sub>3</sub> powders in a 20 mL of ethanol of 2 x 10<sup>-2</sup> M Cd(CH<sub>3</sub>COO)<sub>2</sub>·2H<sub>2</sub>O for 1 day, followed by sulfurization with a 20 mL of ethanol of 2 x 10<sup>-2</sup> M Na<sub>2</sub>S for 1 day. Composite samples were collected by filtration, which was followed by washing and subsequent drying.

Elemental nickel (Ni) and NiO (0.1~3.6 wt %) was loaded on the surface of KNbO<sub>3</sub> by a method that Domen and coworkers<sup>23,53,54</sup> reported. KNbO<sub>3</sub> samples were suspended in a Ni(NO<sub>3</sub>)<sub>2</sub> aqueous solution for 1 day, followed by it being filtered, washed, and dried. The solid was reduced in H<sub>2</sub> atmosphere at 500 °C for 2 h, and subsequently oxidized in an O<sub>2</sub> atmosphere at 200 °C for 1 h. In the case of elemental Ni-loaded KNbO<sub>3</sub> samples (Ni/KNbO<sub>3</sub>), the O<sub>2</sub> oxidation step was eliminated. The NiO-loaded KNbO<sub>3</sub> samples (NiO/KNbO<sub>3</sub>) were obtained by complete O<sub>2</sub> oxidation at 500 °C for 1 h. A schematic flow chart is shown in Figure 4.1.

## Characterization

The crystal structures of synthesized  $\text{KNbO}_3$  samples were confirmed by a powder X-ray diffraction (XRD) using a Phillips diffractometer (X'pert Pro) with  $\text{Cu-K}\alpha$  radiation. Diffuse reflectance spectra were obtained with UV-vis spectrometer (Shimadzu UV-2101PC) and were converted from reflection to absorption spectra by the Kubelka-Munk method. Brunauer-Emmett-Teller (BET) surface area analyses were also performed to compare the surface areas of  $\text{KNbO}_3$  samples that were prepared under different conditions. Microstructures and composition were also analyzed with a LEO 1550VP Field Emission Scanning Electron Microscope (SEM) and Philips EM201 Transmission Electron Microscope (TEM). Inductivity Coupled Plasma-Mass Spectrometry (HP 4500 ICP-MS) was used to determine the amounts of  $\text{Ni}^{2+}$  and  $\text{Cd}^{2+}$  adsorbed on the surface of  $\text{KNbO}_3$ . Pottassium ions released from  $\text{KNbO}_3$  during ion-exchange with  $\text{Ni}^{2+}$  were determined by Dionex DX-500 Ion Chromatography system. X-ray Photoelectron Spectroscopy (XPS) was used to observe the changes in the oxidation state of Nb species and Ni species adsorbed on the surface of  $\text{KNbO}_3$  with Al  $\text{K-}\alpha$  radiation.

## Photocatalytic Reaction

Photocatalytic reactions for hydrogen production were carried out in an air-tight reactor vessel under visible light irradiation ( $\lambda > 400 \text{ nm}$ ). Catalyst samples (0.2 g) were suspended in 50 mL of a water/isopropanol mixture (30 v/v %) in a Pyrex glass reactor. Samples were purged with Ar or  $\text{N}_2$  gas for 30 min before reaction in order to eliminate dissolved  $\text{O}_2$ . A high-pressure 500 W Hg-Xe arc lamp in combination with a 400 nm cut-off filter was used as the primary light source. The intensity of incident

light was determined by ferrioxalate actinometry to obtain quantum yields for H<sub>2</sub> production. The amount of H<sub>2</sub> evolved during photolysis was analyzed by GC/TCD (HP 5890, N<sub>2</sub> carrier) with a molecular sieve column (30 m × 0.32 mm × 12.00 μm).

## Results and Discussion

### Ni/NiO/KNbO<sub>3</sub>/CdS Nanocomposite Characterization

Figure 4.2 shows XRD patterns of synthesized KNbO<sub>3</sub> under different calcination temperatures and mole ratios. XRD pattern for KNbO<sub>3</sub> calcined at 925°C with 1:1 mole ratio of K:Nb (Figure 4.2(a)) shows exactly same 2θ peaks that correspond to standard KNbO<sub>3</sub>. Samples calcined over the range of temperature from 650 to 925°C also show the same peak patterns. However, a sample produced at 1025 °C with 1:1.1 mole ratio of K:Nb (Figure 4.2(b)) has an extra 2θ peaks that are attributed to potassium hexaniobate (K<sub>4</sub>Nb<sub>6</sub>O<sub>17</sub>). K<sub>4</sub>Nb<sub>6</sub>O<sub>17</sub> has a perovskite structure similar to KNbO<sub>3</sub>, but it consists of a layered structure composed of two different types of niobate sheets. The material structures are also confirmed by SEM images. A layered structure is only observed for the sample calcined at 1025°C by SEM as shown in Figure 4.3. The diffraction peaks of KNbO<sub>3</sub> samples are more intense and sharper, with an increase in calcination temperature. The broadening of XRD peaks at low calcination temperatures may be due to smaller crystallite size. The particle sizes of KNbO<sub>3</sub> at different calcination temperatures can be estimated with the Scherrer equation; the estimated particle sizes were 28, 32, and 39 nm for KNbO<sub>3</sub> samples prepared at 650 °C, 775 °C and 925 °C, respectively. BET surface areas were also measured at 4.35, 3.08, and 2.14 m<sup>2</sup>g<sup>-1</sup> for 650 °C, 775 °C, and 925 °C samples, respectively, and it is apparent that the

specific surface area decreases with an increase in calcination temperature. Furthermore, there appears to be no observable structural difference between  $\text{KNbO}_3$  samples before and after Ni deposition or with the addition of nanoparticulate CdS. Figure 4.4 is the TEM picture of nanocomposite sample of Ni/NiO/ $\text{KNbO}_3$ /CdS which shows that Ni or CdS nanoparticles were loaded on the surface of  $\text{KNbO}_3$ .

Figure 4.5 shows the light absorption properties of nanocomposite samples. The  $\text{KNbO}_3$ /CdS nanocomposite absorbs visible light at  $\lambda > 400$  nm. This is primarily due to the band gap excitation of Q-size CdS, since  $\text{KNbO}_3$  does not absorb visible light. The respective band gaps are estimated to be 3.4 eV and 2.6 eV for  $\text{KNbO}_3$  and Q-CdS, from the plots of Kubelka-Munk functions vs. photon energy. It should be noted that absorption edge of Q-size CdS synthesized for CdS/ $\text{KNbO}_3$  nanocomposite is blue-shifted from absorption edge of bulk CdS particles.<sup>43</sup>

The synthesized  $\text{KNbO}_3$  samples were suspended in an aqueous  $\text{Ni}(\text{NO}_3)_2$  solution for 1 day to load  $\text{Ni}^{2+}$  as a co-catalyst. ICP-MS and IC results show that most of  $\text{Ni}^{2+}$  ions are adsorbed on the surface of  $\text{KNbO}_3$  particles and some of them are ion-exchanged with  $\text{K}^+$  ions located in  $\text{KNbO}_3$  framework. However, in synthesis of CdS nanoparticle on  $\text{KNbO}_3$  surface, only 20~30% of  $\text{Cd}^{2+}$  ions are adsorbed on the surface and ion exchange with  $\text{K}^+$  are not observed. Then  $\text{Ni}^{2+}$ -adsorbed (or ion-exchanged)  $\text{KNbO}_3$  samples were treated under proper conditions, i.e.,  $\text{H}_2$  reduction at 500 °C followed by  $\text{O}_2$  oxidation at 200 °C. After thermal reduction by  $\text{H}_2$ , the doped samples turned gray from the initial white undoped  $\text{KNbO}_3$ . However, oxidation at 500 °C converts elemental nickel to NiO with a corresponding change in color from gray to light yellow. XPS analysis of the various samples was used to identify the oxidation states of Ni in each sample.



## Photocatalytic H<sub>2</sub> production

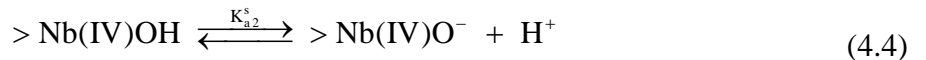
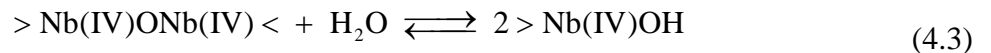
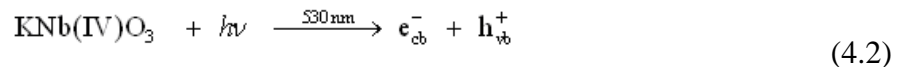
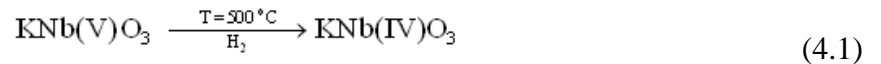
The measured H<sub>2</sub> production rates in illuminated aqueous isopropanol solutions under visible light with CdS, KNbO<sub>3</sub>, Ni/NiO/KNbO<sub>3</sub>, and Ni/NiO/KNbO<sub>3</sub>/CdS composites are compiled in Table 4.1. The naked KNbO<sub>3</sub>, nickel-doped KNbO<sub>3</sub>, and Ni/NiO/KNbO<sub>3</sub> samples showed no activity for H<sub>2</sub> production under the visible light since its band gap energy (3.4 eV) was larger than the excitation energies ( $\lambda > 400$  nm). Simple Q-CdS nanoparticle suspensions produce H<sub>2</sub>, but at very low rates. However, H<sub>2</sub> production rates increase significantly in the KNbO<sub>3</sub>/CdS nanocomposites. This may be due to effective charge separation of electrons and holes in illuminated CdS, with electron injection into the conduction band of KNbO<sub>3</sub> possible in the KNbO<sub>3</sub>/CdS nanocomposites. H<sub>2</sub> production with TiO<sub>2</sub> (Degussa P-25)/CdS nanocomposites was also performed for comparison. TiO<sub>2</sub>/CdS had lower H<sub>2</sub> production activity than KNbO<sub>3</sub>/CdS. H<sub>2</sub> production rates for the KNbO<sub>3</sub>/CdS nanocomposites were enhanced significantly in the presence of the deposited Ni/NiO co-catalysts. Ni most likely serves to collect conduction band electrons. However, a significant enhancement of H<sub>2</sub> production rate was not observed in Pt deposited KNbO<sub>3</sub> samples (Pt/KNbO<sub>3</sub>/CdS) as compared to Ni/KNbO<sub>3</sub>/CdS nanocomposites. We also synthesized potassium hexaniobate (K<sub>4</sub>Nb<sub>6</sub>O<sub>17</sub>) for comparison because K<sub>4</sub>Nb<sub>6</sub>O<sub>17</sub> is known as a good photocatalyst for H<sub>2</sub> production under UV light irradiation.<sup>20,22,23</sup> However, the result shows that KNbO<sub>3</sub>/CdS nanocomposite produces more H<sub>2</sub> than K<sub>4</sub>Nb<sub>6</sub>O<sub>17</sub>/CdS under visible light irradiation.

The enhanced reactivity of the KNbO<sub>3</sub> nanocomposites may be due to involvement of the reduced states of niobium and/or oxygen vacancies that allow for the photoexcitation

of mobile electrons with visible light. For example, Ewart et al.<sup>55</sup> reported that mobile electrons are generated in electrochemically reduced and Fe-doped KNbO<sub>3</sub> upon excitation at 532 nm. The electrons photoexcited at 532 nm had lifetimes of 4 ns and electron mobilities of 0.5 cm<sup>2</sup> V<sup>-1</sup> s<sup>-1</sup>. They concluded that the photoexcited electrons are trapped within 4 ns (i.e., loss of detectable mobility), however, the trapped-state electrons are thermally activated on a millisecond timeframe and eventually recombine with the internal donor states. Kesselman et al.<sup>56</sup> observed a similar reduction in Nb<sub>2</sub>O<sub>5</sub>/TiO<sub>2</sub> composites that were reduced over hydrogen at high temperatures. Reduction of Nb<sub>2</sub>O<sub>5</sub> is known to form a variety of phases such as Nb<sub>12</sub>O<sub>29</sub>, Nb<sub>22</sub>O<sub>54</sub>, Nb<sub>25</sub>O<sub>62</sub>, and Nb<sub>47</sub>O<sub>116</sub> that involve partial oxygen loss coupled with the formation of Nb(IV). Therefore, the longer lifetimes ( $\tau_{tr} > \text{ms}$ ) of the trapped electrons may contribute to the higher reduction rates for bound protons or hydroxides. Similar mixed valence state phase should coexist within the framework of reduced KNbO<sub>3</sub> and contribute to the photo-excitation of electrons and to the overall photoactivity with visible light. The Ni/NiO/KNbO<sub>3</sub> samples were thermally treated at 500 °C under H<sub>2</sub> atmosphere to reduce Ni<sup>2+</sup> to elemental nickel. This treatment step may lead to creation of oxygen vacancies or formation of the reduced states (e.g., Nb(IV) and Nb(III) states) of niobium. The thermal treatment of pure, white KNbO<sub>3</sub> at 500 °C under H<sub>2</sub> produced a light gray product that is consistent with Nb(V) reduction. We performed XPS analysis to compare the oxidation states of Nb between KNbO<sub>3</sub> samples before and after H<sub>2</sub> reduction, however, the reduced states were not readily observed. However, it was measured that reduced states of Nb are formed during the photolytic reaction. Another relevant feature of the metal niobates (e.g., LiNbO<sub>3</sub><sup>57</sup> and KNbO<sub>3</sub><sup>58</sup>), which is critical for

electro-optic and photorefractive applications, is the activation of surface protons (i.e., protons bound in hydroxyl ions,  $^-\text{OH}$ ). The hydroxyl bound protons have activation energies in the range of 1 eV for mobility in  $\text{KNbO}_3$  crystals.

In light of the above photophysical properties related to surface hydroxyl groups, an alternative pathway may involve excitation of reduced  $\text{KNbO}_3$  with visible light followed by conduction band reduction of surface bound protons on  $\text{KNbO}_3$ . The pH of zero point of charge,  $\text{pH}_{\text{zpc}}$ , of  $\text{KNbO}_3$  was measured  $\sim \text{pH } 3.2$ , thus  $\text{KNbO}_3$  surface may be dominated by  $>\text{NbOH}$  and  $>\text{NbO}^-$  under our optimal experimental conditions ( $\sim \text{pH } 8$ ). Given this situation, we can write the following set of reactions that may result in  $\text{H}_2$  production on  $\text{KNbO}_3$  surface sites or  $\text{Ni/NiO/KNbO}_3$  composite sites:



In addition, we compared three different procedures for attachment of CdS particles on the  $\text{KNbO}_3$  surface as shown in Figure 4.6. To form  $\text{KNbO}_3/\text{CdS}$  nanocomposites, we first added  $\text{Cd}^{2+}$  ions in  $\text{KNbO}_3$  suspension, and then we added sulfide ( $\text{HS}^-/\text{S}^{2-}$ ) ions after stirring for 1 day (Figure 4.6(a)). ICP-MS results show that only 20~30 % of the Cd in CdS particles are directly synthesized on the  $\text{KNbO}_3$  surface and the remainder of

the CdS particles are suspended freely in the solution. One sample was prepared by mechanical mixing of CdS and KNbO<sub>3</sub> by addition of KNbO<sub>3</sub> after Q-CdS synthesis in ethanol (Figure 4.6(b)) and another sample has only CdS adsorbed on the KNbO<sub>3</sub> surface by removing free Cd<sup>2+</sup> ions in suspension before adding S<sup>2-</sup> ions (Figure 4.6(c)). The CdS surface adsorption sample (Figure 4.6(c)) shows reasonable photoactivity even though the amounts of CdS are quite small (20~30 %) compared to samples having CdS synthesized both on KNbO<sub>3</sub> surface and in solution (Figure 4.6(a)). As a consequence, we conclude that direct CdS contact with the KNbO<sub>3</sub> surface plays an important role for effective charge separation with increased H<sub>2</sub> production rates, although externally mixed sample (Figure 4.6(b)) also has measurable H<sub>2</sub> production rates. From these results, we can infer that Q-CdS particles are attached to the surface of KNbO<sub>3</sub> under our experimental conditions (~ pH 8) even though CdS was synthesized initially in solution phase.

The KNbO<sub>3</sub> surface is negatively charged under the pH conditions of our experiments since the p*H*<sub>zpc</sub> of KNbO<sub>3</sub> is measured ~ pH 3.2. The actual determination of p*H*<sub>zpc</sub> of the nanoparticulate CdS colloids is more difficult. Park and Huang<sup>59</sup> reported a p*H*<sub>zpc</sub> = 7.5 for colloidal CdS based on electrophoretic mobility measurements and acid-base titrations. At an ionic strength of  $\mu = 0.05$  M, they determined that  $\text{p}K_{\text{a}1}^{\text{s}} = 6.1$  and  $\text{p}K_{\text{a}2}^{\text{s}} = 9.0$  for  $[\text{Cd}^{2+}] = 2.5 \mu\text{M}$  and  $\sigma_0 = 20 \text{ mC cm}^{-2}$ . Liu and Huang<sup>60</sup> subsequently reported a p*H*<sub>zpc</sub> for cubic CdS of 7.0 and p*H*<sub>zpc</sub> = 7.5 for hexagonal CdS. In contrast, other researchers<sup>61-63</sup> have reported substantially lower values for the p*H*<sub>zpc</sub> for CdS in aqueous suspensions. Under experimental conditions that were quite different from those employed by Park and Huang,<sup>59</sup> Nicolau et al.<sup>63</sup> determined a p*H*<sub>zpc</sub> = 1.8 for 0.01

M  $\text{Na}_2\text{SO}_4$  and  $\text{KCl}$  as background electrolytes based on electrophoretic mobility measurements. Guindo et al.<sup>62</sup> found even lower values of  $\text{pH}_{\text{zpc}}$  between 1 and 1.5 for spherical  $\text{CdS}$  particles differently prepared. However, they pointed out that the IEP (isoelectric point) was sensitive to the specific surface characteristics of  $\text{CdS}$  that depends on the degree of oxidation or aging as noted by the shift in IEP to higher values for samples that were synthesized over longer periods of time. According to our observations, it may be true that  $\text{pH}_{\text{zpc}}$  of  $\text{CdS}$  is relatively high value under our experimental conditions, so that  $\text{CdS}$  colloid in solution are positively-charged and then electrostatically attracted to the negatively charged  $\text{KNbO}_3$  particles under our experimental pH condition.

The rates of  $\text{H}_2$  production on the four-component composite,  $\text{Ni/NiO/KNbO}_3/\text{CdS}$  are compared to the three-component composite containing only  $\text{Ni}$  or  $\text{NiO}$ . The data presented in Figure 4.7 shows that elemental  $\text{Ni}$  on  $\text{KNbO}_3$  is a more active species than  $\text{NiO}$  on  $\text{KNbO}_3$  to improve  $\text{H}_2$  production, although its external surface is partially oxidized to  $\text{NiO}$ . However, the  $\text{H}_2$  production rates are not greatly enhanced in the three-component composite containing only  $\text{NiO}$ . This tendency is consistent with previous results obtained for  $\text{Ni/NiO}$  loaded onto  $\text{SrTiO}_3$  as reported by Domen et al.<sup>53</sup> They reported that  $\text{Ni/NiO/SrTiO}_3$  produced substantially more  $\text{H}_2$  from aqueous methanol than the simpler  $\text{NiO/SrTiO}_3$  system under UV irradiation. They concluded that the presence of  $\text{Ni}$  metal in contact with the  $\text{SrTiO}_3$  surface plays an important role in the  $\text{H}_2$  production activity. Domen et al.<sup>64</sup> also found small amounts of  $\text{H}_2$  evolved under the band gap irradiation of  $\text{Ni/SrTiO}_3$ . They attributed their low activity to loss of  $\text{Ni}$  by release of  $\text{Ni}^{2+}$  due to oxidation of  $\text{Ni}$  metal by direct hole transfer from  $\text{SrTiO}_3$

during band gap irradiation. In contrast, our results show that the three-component Ni/KNbO<sub>3</sub>/CdS composite can produce a comparable amount of H<sub>2</sub> compared to the four-component Ni/NiO/KNbO<sub>3</sub>/CdS composite. In both the 3- and 4-component catalyst, the primary absorption occurs at  $\lambda > 400$  nm (compared to SrTiO<sub>3</sub> with  $\lambda < 400$  nm) with CdS as a chromophore. Thus, elemental nickel deposited on KNbO<sub>3</sub> is unlikely to be directly oxidized by holes in our composite material.

As shown in Table 4.1, the highest H<sub>2</sub> production rates were obtained with a Ni-deposition level of 0.1 wt. % as (Ni<sub>T</sub> = Ni + NiO), and above this level, enhancement due to nickel deposition was marginal. However, we observed the enhanced H<sub>2</sub> production with higher wt% of Ni deposition on KNbO<sub>3</sub> samples prepared at low calcination temperatures. The increase of photoactivities with 0.5 ~ 1.0 wt. % Ni-loaded on KNbO<sub>3</sub> prepared at low calcination temperatures may be only due to a simple increase in the total reactive surface area. It is noted that KNbO<sub>3</sub> sample mixed with K<sub>4</sub>Nb<sub>6</sub>O<sub>17</sub> structure which was calcined at 1025°C produces comparable amounts of H<sub>2</sub> to KNbO<sub>3</sub> samples calcined at 925°C.

We observed fairly dramatic color changes taking place during irradiation of the Q-size CdS and the CdS nanocomposite materials. In all cases, the catalysts suspensions are yellow before illumination because of CdS chromophore. However, after exposure to a focused beam of light at  $\lambda > 400$  nm, the color changes very quickly to a silver gray. As the color changes from yellow to gray, H<sub>2</sub> production is observed as a steady stream of gas bubbles rising up in the photolysis cell. The observed color change may be due to the rapid photoreduction of Cd(II) to Cd(I) and then to Cd(0) on the surface of CdS in the absence of oxygen. There is also some probability that S(-II) in the CdS matrix is

also oxidized partially by trapped valence band holes to form S(0) and eventually polysulfide ion ( $S_2^{2-}$ ). Upon exposure to oxygen, the yellow color is regenerated over several hours with the return of yellow CdS on the nanocomposite structures.

Apparent quantum yields,  $\phi$ , for  $H_2$  production, were determined as follows:

$$\phi = \frac{\frac{dm_{H_2}}{dt}}{I_{abs}^o} \times 2 \quad (4.7)$$

where  $dm_{H_2}/dt$  is an initial production rate of  $H_2$  ( $mol\ s^{-1}$ ) and  $I_{abs}^o$  is photon absorption rate in units of Einstein  $s^{-1}$  ( $mol(e^-)\ s^{-1}$ ). We also considered the fact that two electrons are consumed to produce one hydrogen molecule from two protons for quantum yield calculation. The photon flux through the cell was  $2.3 \times 10^{17}$  photons  $s^{-1}$ , as determined by ferrioxalate actinometry with an apparent quantum yield for  $H_2$  production of 4.4 % for  $\lambda > 400$  nm. It should be noted that the amount of light scattered from nanocomposites suspension was not considered here and therefore actual quantum yield may be higher.

### **Photocatalytic $H_2$ Production Under Natural Sunlight**

Substantial amounts of hydrogen gas are also produced readily using natural sunlight as the irradiation source. For example, the 4-composite was exposed to solar light between 11:30 am and 3:30 pm on the roof of W. M. Keck Laboratories at Caltech on August 13, 2006. Experimental procedures were identical to those employed in the controlled laboratory experiments except for the use of different types of pyrex reactors. As shown in Figure 4.8,  $H_2$  is readily produced from aqueous isopropanol solutions under natural sunlight; however, the amount of  $H_2$  produced is actually larger than that

produced over the same period of time under UV light irradiation in the laboratory. This simple demonstration illustrates the potential of practical application of Ni/NiO/KNbO<sub>3</sub>/CdS nanocomposite for H<sub>2</sub> production with sunlight.

### **Influence of Solvent Composition on Photocatalytic H<sub>2</sub> Production**

The relative effects of a variation of solvent/water mixtures on H<sub>2</sub> production for KNbO<sub>3</sub>/CdS at  $\lambda > 400$  nm are illustrated as shown in Figure 4.9. 30 v/v% of isopropanol (IPA), ethanol (EtOH), and methanol (MeOH) solution were used in the photoreaction. The order of photoreactivity is IPA > EtOH > MeOH, which is in inverse order of their dielectric constants (i.e.,  $\epsilon_{\text{IPA}} = 19 < \epsilon_{\text{EtOH}} = 24.3 < \epsilon_{\text{MeOH}} = 33$ ).

Alcohols function primarily as hole traps that prevent rapid electron-hole recombination. The presence of an electron donor other than water is crucial for photocatalytic H<sub>2</sub> production, since little H<sub>2</sub> is produced without added electron donors even under UV light irradiation. However, the interaction of the various electron donors with the charged CdS surface will also depend on their chemical and physical properties. Alcohols have substantially lower dielectric constants than H<sub>2</sub>O ( $\epsilon = 80.4$ ). As a consequence, we predict that the relative thickness of the electrical double layer (EDL) should decrease when alcohols are added. The EDL thickness should decrease in the order of dielectric constants, as given by the Debye equation:

$$\kappa \equiv \left( \frac{2 F^2 \mu}{\epsilon \epsilon_0 R T} \right)^{0.5} \quad (4.8)$$

where  $\epsilon$  is the dielectric constant of the solvent or mixed solvent system,  $\epsilon_0$  is the permittivity of free space ( $8.854 \times 10^{-12} \text{ C}^2 \text{ J}^{-1} \text{ m}^{-1}$ ),  $\mu$  is the ionic strength of the



background electrolyte ( $\text{mol m}^{-3}$ ),  $R$  is the gas constant ( $8.314 \text{ J mol}^{-1} \text{ K}^{-1}$ ),  $T$  is temperature in units of  $\text{K}$ , and  $F$  is the Faraday constant ( $96485 \text{ C mol}^{-1}$ ). Electrical double layer compression will enhance the physicochemical interaction of the electron donors with the charged CdS surface. Thus, a more efficient hole trapping by the electron donors should increase  $\text{H}_2$  production rates.

We note that  $\text{SO}_3^{2-}$  and  $\text{S}^{2-}$  are also frequently used as sacrificial donors to prevent the photocorrosion of metal sulfide semiconductors;<sup>19,46,47,65</sup> however, the  $\text{H}_2$  production rate of  $\text{KNbO}_3/\text{CdS}$  nanocomposites with the addition of  $0.01 \text{ M SO}_3^{2-}$  and  $0.1 \text{ M S}^{2-}$  was very low relative to adding alcohols as electron donors.

### **Influence of pH on Photocatalytic $\text{H}_2$ Production**

Without the addition of acid or base, the pH of the  $\text{KNbO}_3/\text{CdS}$  suspensions in  $\text{ROH}/\text{H}_2\text{O}$  is between pH 8 and 9. The pH-dependent production of  $\text{H}_2$  from aqueous isopropanol solution under visible light is shown in Figure 4.10. The highest production rates of  $\text{H}_2$  were obtained in the circumneutral pH region, while the rates of  $\text{H}_2$  production decreased at higher and lower pH.

The relative attachment of Q-CdS on the  $\text{KNbO}_3$  particles should be influenced by the  $\text{KNbO}_3$  and CdS surface charges. Since the  $\text{pH}_{\text{zpc}}$  value of  $\text{KNbO}_3$  was determined to be 3.2, the  $\text{KNbO}_3$  surface is negatively charged at both neutral and alkaline pH (i.e.,  $\text{pH} > \text{pH}_{\text{zpc}}$ ) and is positively charged at very acidic pH (i.e.  $\text{pH} < \text{pH}_{\text{zpc}}$ ). In case of Q-CdS,  $\text{pH}_{\text{zpc}}$  value varies from pH 1 to 7, according to the structure and surface characteristics of CdS, and the types and concentrations of background electrolytes. However, we assume that the  $\text{pH}_{\text{zpc}}$  of CdS is more likely to be high under our conditions to possibly account

for the rapid attachment of CdS colloids to the larger KNbO<sub>3</sub> particles (Figure 4.6(c)). Therefore, at circumneutral pH, positively charged CdS can be adsorbed onto the negatively charged KNbO<sub>3</sub> surface. At low pH, the surface charges of CdS and KNbO<sub>3</sub> would be positive, and at high pH, both particles are negatively charged so that effective contact and charge transfer from CdS to KNbO<sub>3</sub> is less likely to occur at extreme pH. Furthermore, proton ion-exchange also occurs for KNbO<sub>3</sub> samples under acidic conditions. K<sup>+</sup> ions in the framework of KNbO<sub>3</sub> may be ion-exchanged with H<sup>+</sup> ions, and a proton-exchanged form, K<sub>1-x</sub>H<sub>x</sub>NbO<sub>3</sub>, may have different structure and physicochemical properties from the original KNbO<sub>3</sub> materials. We prepared K<sub>1-x</sub>H<sub>x</sub>NbO<sub>3</sub> samples by stirring in 0.5 N H<sub>2</sub>SO<sub>4</sub> solutions for several days followed by washing, filtration, and drying, and tested photoactivity of K<sub>1-x</sub>H<sub>x</sub>NbO<sub>3</sub>/CdS nanocomposites for H<sub>2</sub> production. In circumneutral pH region, K<sub>1-x</sub>H<sub>x</sub>NbO<sub>3</sub>/CdS nanocomposites show extremely low H<sub>2</sub> production rates (~ 2.8 μmol h<sup>-1</sup>g<sup>-1</sup>). Therefore, we conclude that proton-exchanged KNbO<sub>3</sub> can be formed in low pH and it may cause low photoactivity of KNbO<sub>3</sub> for H<sub>2</sub> production in acidic pH.

## Conclusions

Efficient H<sub>2</sub> production was obtained with Ni/NiO/KNbO<sub>3</sub>/CdS composites with visible light irradiation ( $\lambda > 400$  nm). H<sub>2</sub> production rates were higher than TiO<sub>2</sub>/CdS or K<sub>4</sub>Nb<sub>6</sub>O<sub>17</sub>/CdS composites. Partially reduced states of niobium (e.g., Nb(IV) and Nb(III)), which are generated during Ni formation under H<sub>2</sub> and by photoreduction, may contribute to the enhanced reactivity of the KNbO<sub>3</sub> composites. Aliphatic alcohols (methanol, ethanol, isopropanol, etc.) serve as alternative electron donors and modified

the near surface environment via electrical double layer compression. The solution pH also influences the rate of photocatalytic H<sub>2</sub> production, with the highest H<sub>2</sub> production rates obtained at circumneutral pH. In addition, the 4-component nanocomposite (Ni/NiO/KNbO<sub>3</sub>/CdS) produces H<sub>2</sub> rapidly under natural sunlight. Our findings suggest that use of solar energy for photocatalytic water splitting with this developed photocatalyst system may give a promising source for hydrogen fuel.

### **Acknowledgement**

We are grateful to the Hydrogen Energy Research & Development Center and 21<sup>st</sup> Century Frontier Research and Development Program of the Ministry of Science and Technology of Korea for research support.

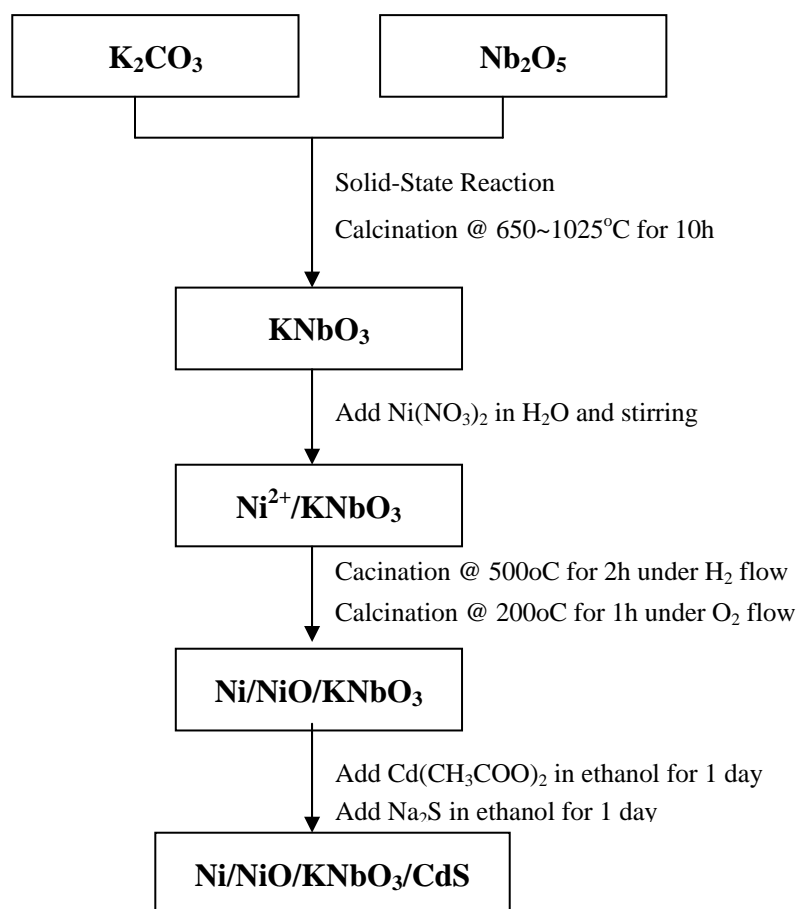


**Figure 4.1.** Schematic flow chart outlining the synthetic procedures for the composite Ni/NiO/  $\text{KNbO}_3/\text{CdS}$  catalyst preparation

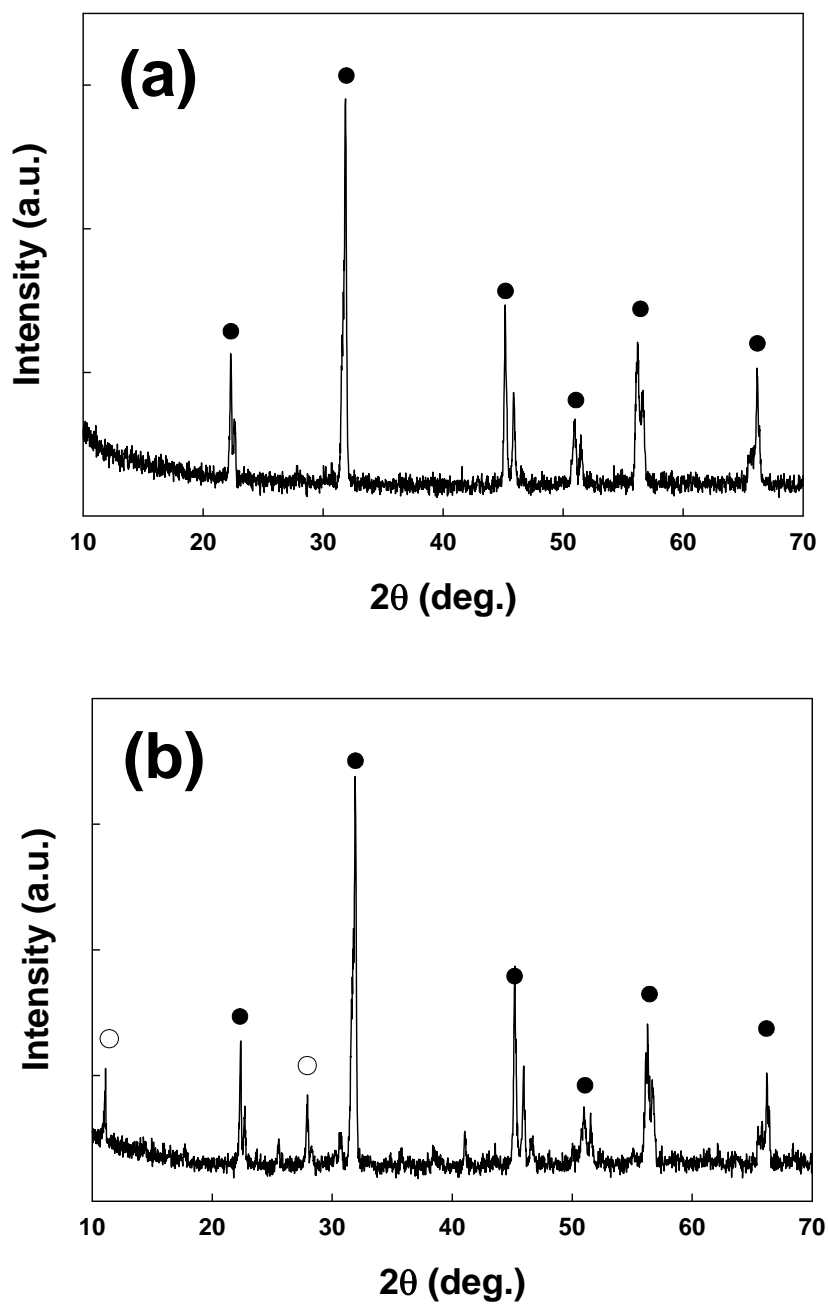


**Figure 4.2.** X-ray diffraction pattern for (a)  $\text{KNbO}_3$  powder sample synthesized from 1:1 mole ratio of  $\text{Nb}_2\text{O}_5$  and  $\text{K}_2\text{CO}_3$  at  $925^\circ\text{C}$  and (b)  $\text{KNbO}_3$  powder sample synthesized from 1:1.1 mole ratio of  $\text{Nb}_2\text{O}_5$  and  $\text{K}_2\text{CO}_3$  at  $1025^\circ\text{C}$ . ( $\bullet$ )  $\text{KNbO}_3$ , ( $\circ$ )  $\text{K}_4\text{Nb}_6\text{O}_{17}$

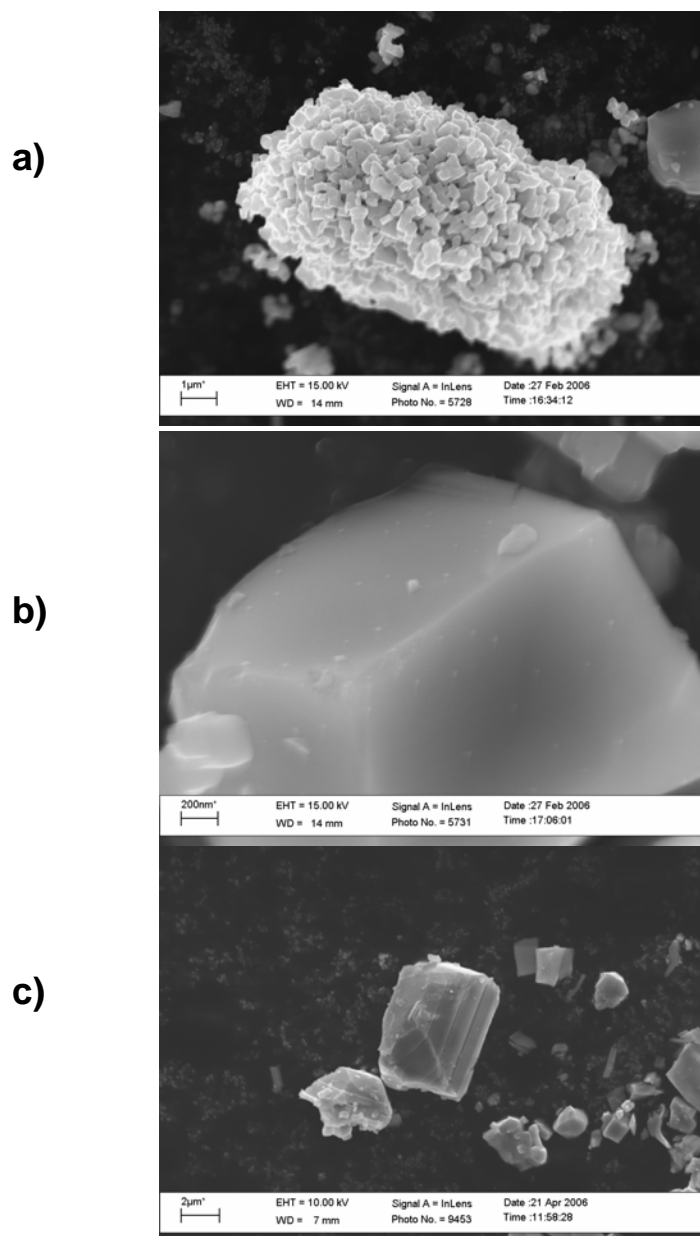


**Figure 4.3.** SEM images of (a), (b)  $\text{KNbO}_3$  synthesized at  $925^\circ\text{C}$  (K:Nb=1:1) and (c)  $\text{KNbO}_3$  synthesized at  $1025^\circ\text{C}$  (K:Nb = 1:1.1)

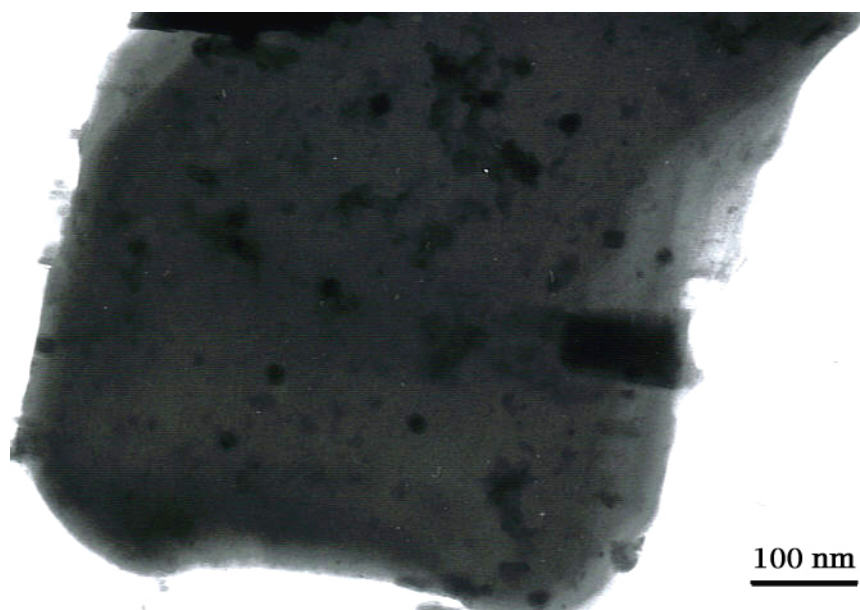


**Figure 4.4.** TEM images of Ni/NiO/KNbO<sub>3</sub>/CdS nanocomposite

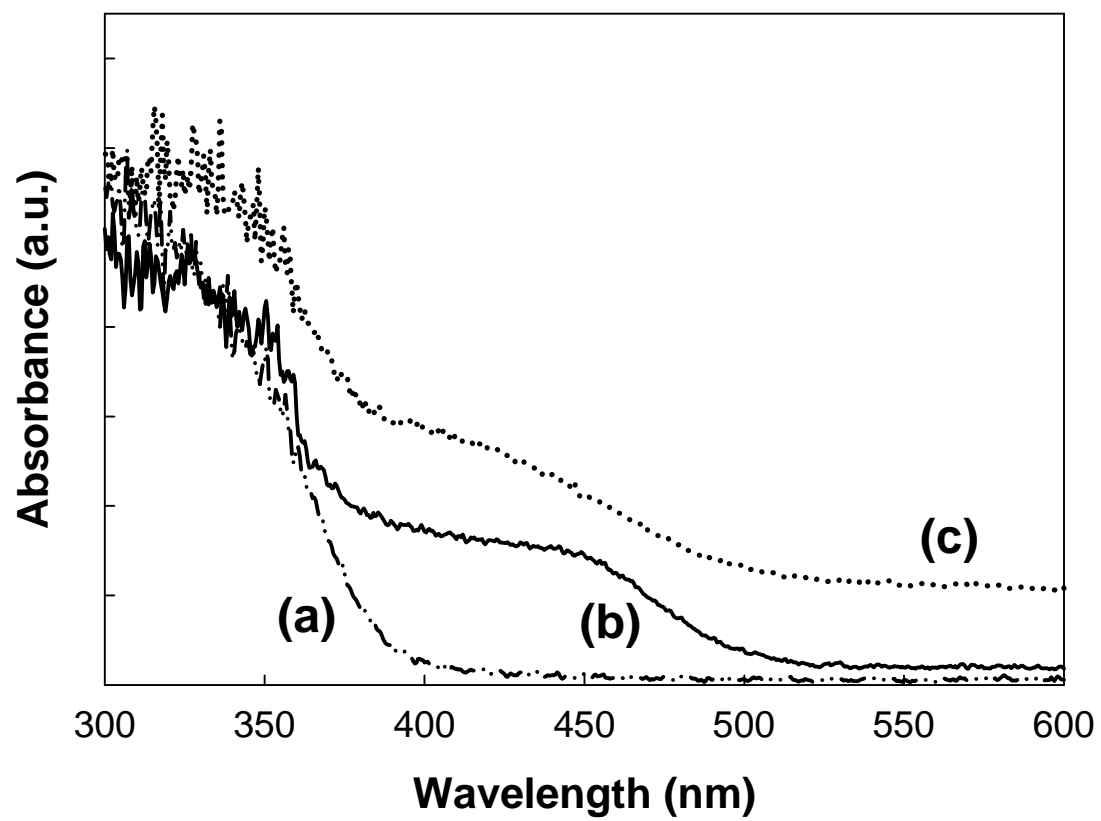


**Figure 4.5.** UV-vis diffuse reflectance spectra for (a)  $\text{KNbO}_3$ , (b)  $\text{KNbO}_3/\text{CdS}$ , (c)  $\text{Ni/NiO/KNbO}_3/\text{CdS}$



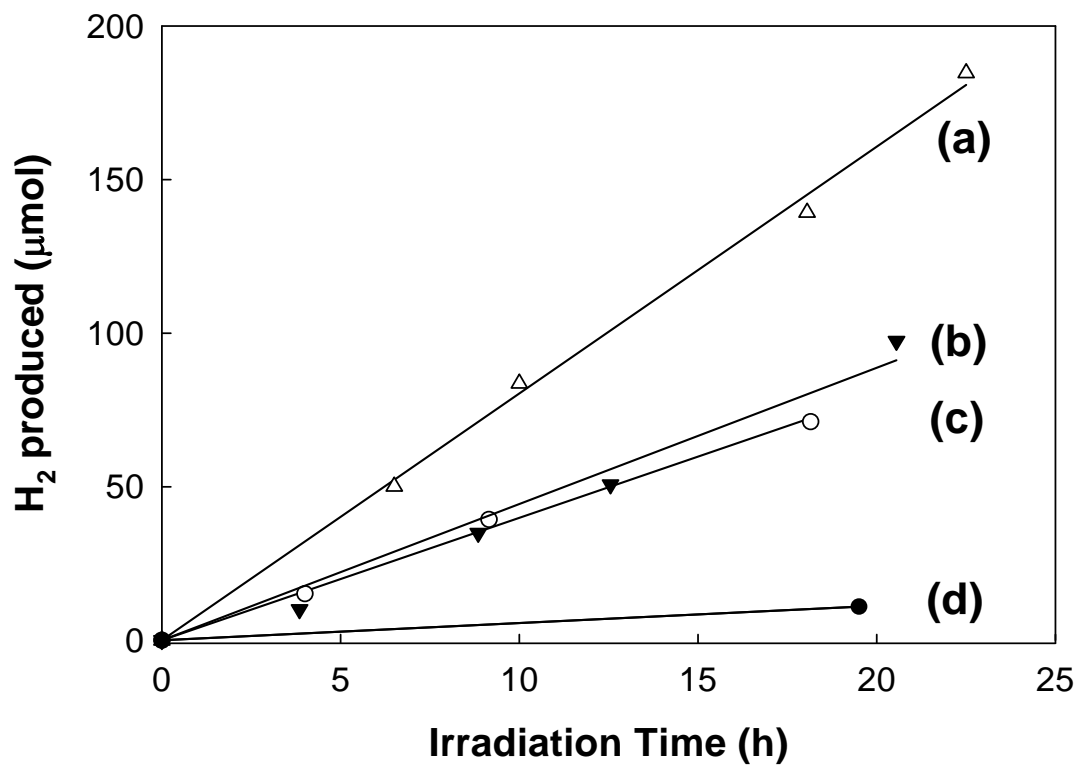


**Figure 4.6.** Effect of CdS loading on KNbO<sub>3</sub> surface on photocatalytic activities for H<sub>2</sub> production: (a) CdS synthesized both on KNbO<sub>3</sub> surface and in solution, (b) CdS synthesized by external mixing with KNbO<sub>3</sub>, (c) CdS adsorbed on KNbO<sub>3</sub>, (d) Q-size CdS only

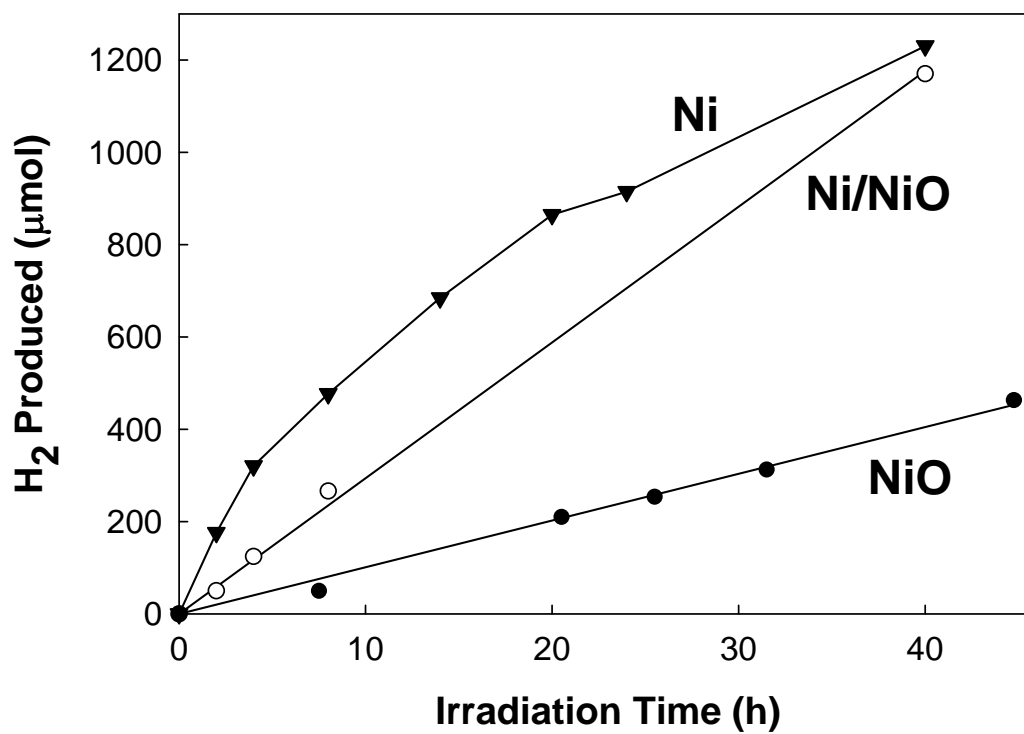


**Figure 4.7.** Effect of oxidation states of Ni deposited  $\text{KNbO}_3$  (0.1 wt % loading as  $\text{Ni}_T$ ) on photocatalytic  $\text{H}_2$  production from water-isopropanol mixed solution

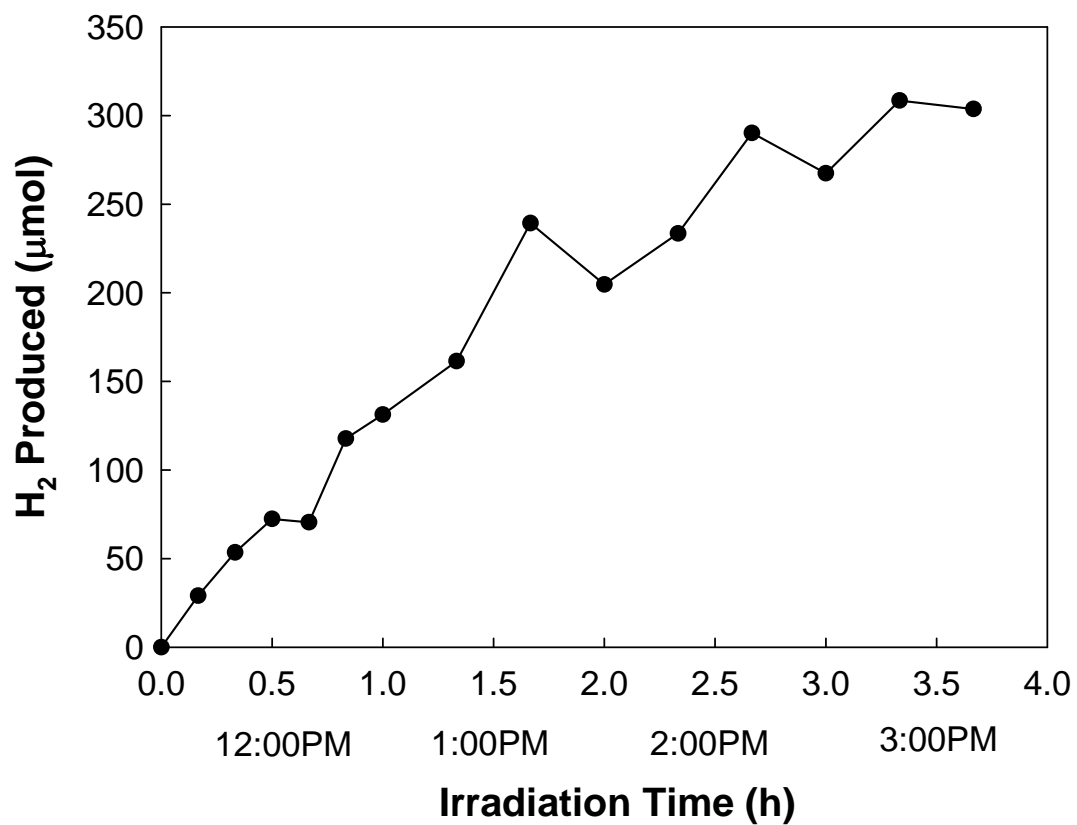


**Figure 4.8.** H<sub>2</sub> production rate from water-isopropanol mixed solution with Ni/NiO/KNbO<sub>3</sub>/CdS under natural sunlight (August 13, 2006; Pasadena, California).\

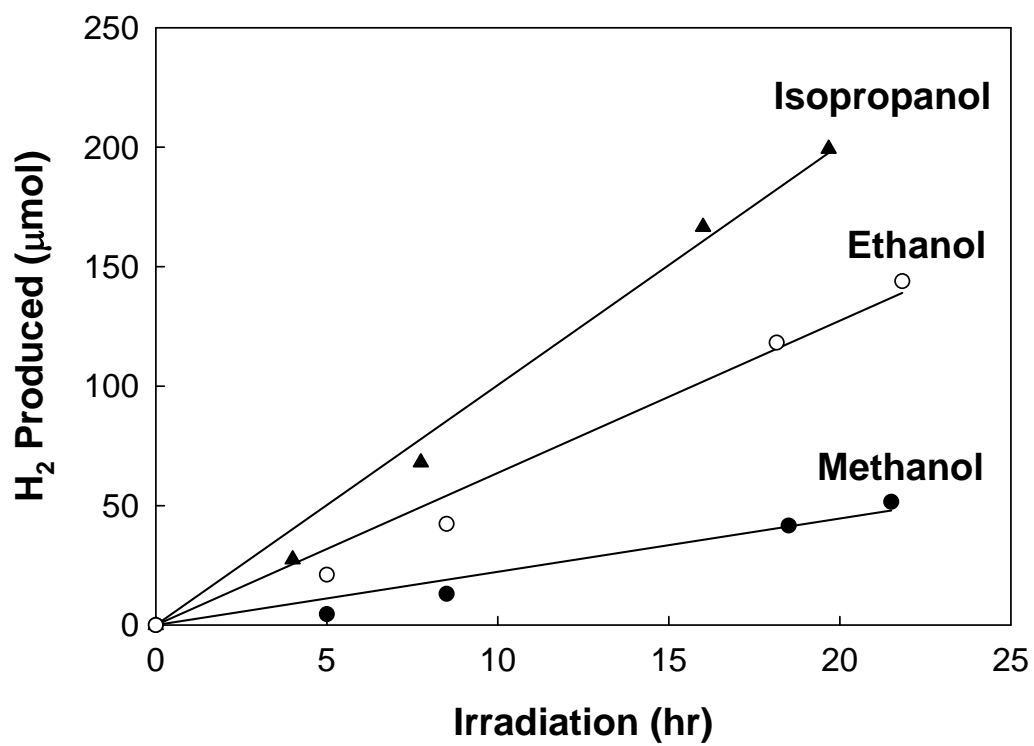


**Figure 4.9.** Solvent effects on photocatalytic H<sub>2</sub> production with Ni/NiO/KNbO<sub>3</sub>/CdS under the visible light ( $\lambda > 400\text{nm}$ )

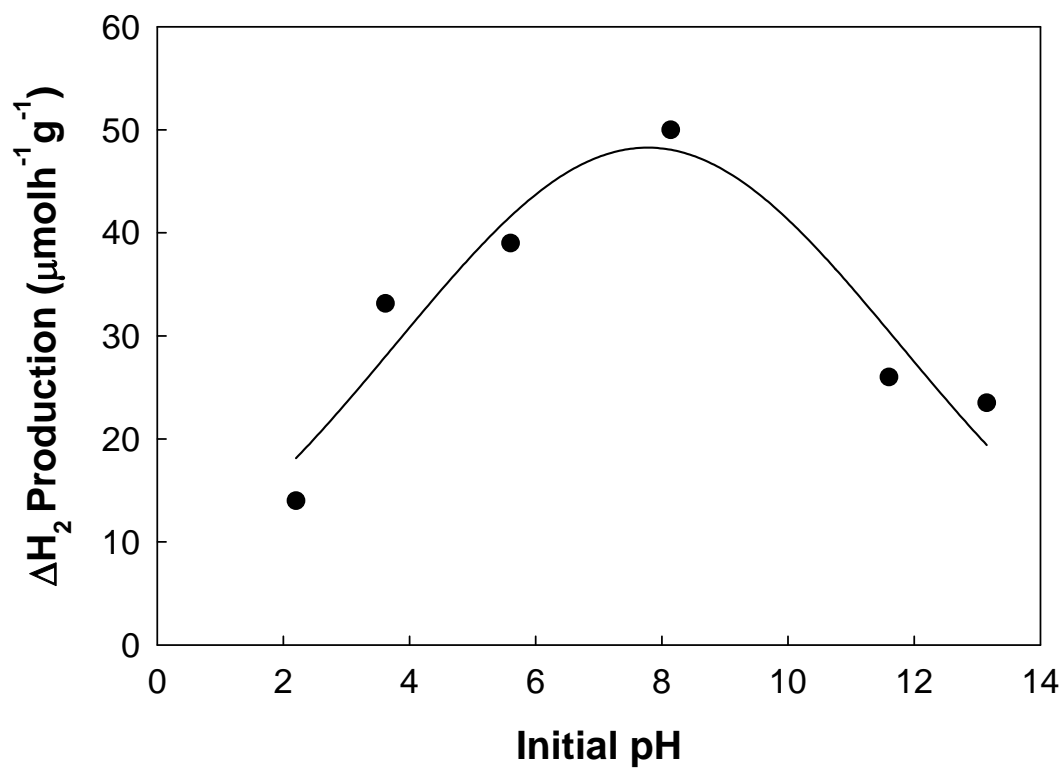


**Figure 4.10.** pH-dependent  $H_2$  production from water-isopropanol mixed solution. pH was adjusted with 0.1~1 M NaOH and HCl.

**TABLE 4.1.** Photocatalytic activities of potassium niobates nanocomposites for H<sub>2</sub> production from water-isopropanol mixed solution

Sample	weight % of Ni <sub>T</sub>	Calcination Temp. (°C)	H <sub>2</sub> Production <sup>a</sup> (μmolh <sup>-1</sup> g <sup>-1</sup> )
KNbO <sub>3</sub>	0	925	0
Ni/NiO/KNbO <sub>3</sub>	0.1	925	0
CdS	0	-	3
TiO <sub>2</sub> /CdS	0	-	12
Ni/NiO/K <sub>4</sub> Nb <sub>6</sub> O <sub>17</sub> /CdS	0.1	1150	37
Ni/NiO/KNbO <sub>3</sub> /CdS	0	925	50
	0.1	925	150
	0.3	925	125
	0.5	925	75
	1.0	925	80
	3.6	925	65
	0.5	650	110
	0.5	775	80
	1.0	650	120
	1.0	775	80

<sup>a</sup> Catalyst, 0.2 g; volume, 50 ml; light source, Hg-Xe lamp (500W) with λ > 400nm, 30 v/v% isopropanol

## References

- (1) Fujishima, A.; Honda, K. *Nature* **1972**, *238*, 37.
- (2) Karakitsou, K. E.; Verykios, X. E. *J. Catal.* **1992**, *134*, 629.
- (3) Sakata, T.; Kawai, T. *Chem. Phys. Lett.* **1981**, *80*, 341.
- (4) Abe, R.; Takata, T.; Sugihara, H.; Domen, K. *Chem. Commun.* **2005**, 3829.
- (5) Gondal, M. A.; Hameed, A.; Yamani, Z. H. *Energy Sources* **2005**, *27*, 1151.
- (6) Hwang, D. W.; Kim, J.; Park, T. J.; Lee, J. S. *Catal. Lett.* **2002**, *80*, 53.
- (7) Domen, K.; Naito, S.; Onishi, T.; Tamaru, K. *Chem. Phys. Lett.* **1982**, *92*, 433.
- (8) Zou, J. J.; Liu, C. J. *Acta Physico-Chimica Sinica* **2006**, *22*, 926.
- (9) Hoffman, A. J.; Yee, H.; Mills, G.; Hoffmann, M. R. *J. Phys. Chem.* **1992**, *96*, 5540.
- (10) Maeda, K.; Takata, T.; Hara, M.; Saito, N.; Inoue, Y.; Kobayashi, H.; Domen, K. *J. Am. Chem. Soc.* **2005**, *127*, 8286.
- (11) Steinfeld, A. *Int. J. Hydrogen Energy* **2002**, *27*, 611.
- (12) Ashokkumar, M. *Int. J. Hydrogen Energy* **1998**, *23*, 427.
- (13) De, G. C.; Roy, A. M.; Bhattacharya, S. S. *Int. J. Hydrogen Energy* **1996**, *21*, 19.
- (14) Furlong, D. N.; Grieser, F.; Hayes, D.; Hayes, R.; Sasse, W.; Wells, D. *J. Phys. Chem.* **1986**, *90*, 2388.
- (15) Guan, G. Q.; Kida, T.; Kusakabe, K.; Kimura, K.; Fang, X. M.; Ma, T. L.; Abe, E.; Yoshida, A. *Chem. Phys. Lett.* **2004**, *385*, 319.
- (16) Kakuta, N.; Park, K. H.; Finlayson, M. F.; Ueno, A.; Bard, A. J.; Campion, A.; Fox, M. A.; Webber, S. E.; White, J. M. *J. Phys. Chem.* **1985**, *89*, 732.

- (17) Muradov, N. Z.; Rustamov, M. I.; Guseinova, A. D.; Bazhutin, Y. V. *React. Kinet. Catal. Lett.* **1987**, *33*, 279.
- (18) Kobayashi, J.; Kitaguchi, K.; Tanaka, H.; Tsuiki, H.; Ueno, A. *J. Chem. Soc., Faraday Trans. I* **1987**, *83*, 1395.
- (19) Koca, A.; Sahin, M. *Int. J. Hydrogen Energy* **2002**, *27*, 363.
- (20) Domen, K.; Kudo, A.; Shibata, M.; Tanaka, A.; Maruya, K.; Onishi, T. *J. Chem. Soc., Chem. Commun.* **1986**, 1706.
- (21) Furube, A.; Shiozawa, T.; Ishikawa, A.; Wada, A.; Domen, K.; Hirose, C. *J. Phys. Chem. B* **2002**, *106*, 3065.
- (22) Ikeda, S.; Tanaka, A.; Shinohara, K.; Hara, M.; Kondo, J. N.; Maruya, K. I.; Domen, K. *Microporous Mater.* **1997**, *9*, 253.
- (23) Sayama, K.; Tanaka, A.; Domen, K.; Maruya, K.; Onishi, T. *Catal. Lett.* **1990**, *4*, 217.
- (24) Sayama, K.; Tanaka, A.; Domen, K.; Maruya, K.; Onishi, T. *J. Phys. Chem.* **1991**, *95*, 1345.
- (25) Ikeda, S.; Fubuki, M.; Takahara, Y. K.; Matsumura, M. *Appl. Catal., A* **2006**, *300*, 186.
- (26) Kato, H.; Kudo, A. *J. Phys. Chem. B* **2001**, *105*, 4285.
- (27) Machida, M.; Mitsuyama, T.; Ikeue, K.; Matsushima, S.; Arai, M. *J. Phys. Chem. B* **2005**, *109*, 7801.
- (28) Machida, M.; Yabunaka, J.; Kijima, T. *Chem. Mater.* **2000**, *12*, 812.
- (29) Kim, S.; Hwang, S. J.; Choi, W. Y. *J. Phys. Chem. B* **2005**, *109*, 24260.
- (30) Wang, D. F.; Ye, J. H.; Kako, T.; Kimura, T. *J. Phys. Chem. B* **2006**, *110*, 15824.



- (31) Gu, D. E.; Yang, B. C.; Hu, Y. D. *Catal. Lett.* **2007**, *118*, 254.
- (32) Gole, J. L.; Stout, J. D.; Burda, C.; Lou, Y. B.; Chen, X. B. *J. Phys. Chem. B* **2004**, *108*, 1230.
- (33) Kisch, H.; Sakthivel, S.; Janczarek, M.; Mitoraj, D. *J. Phys. Chem. C* **2007**, *111*, 11445.
- (34) Reyes-Gil, K. R.; Reyes-Garcia, E. A.; Raftery, D. *J. Phys. Chem. C* **2007**, *111*, 14579.
- (35) Yin, S.; Komatsu, M.; Zhang, Q. W.; Saito, F.; Sato, T. *J. Mater. Sci.* **2007**, *42*, 2399.
- (36) Murakami, Y.; Kasahara, B.; Nosaka, Y. *Chem. Lett.* **2007**, *36*, 330.
- (37) Yu, J. C.; Ho, W. K.; Yu, J. G.; Yip, H.; Wong, P. K.; Zhao, J. C. *Environ. Sci. Technol.* **2005**, *39*, 1175.
- (38) Liu, H.; Imanishi, A.; Nakato, Y. *J. Phys. Chem. C* **2007**, *111*, 8603.
- (39) Zhang, W. U.; Zhong, Y.; Fan, J.; Sun, S. Q.; Tang, N.; Tan, M. Y.; Wu, L. M. *Sci. China Ser. B* **2003**, *46*, 196.
- (40) Linkous, C. A.; Muradov, N. Z.; Ramser, S. N. *Int. J. Hydrogen Energy* **1995**, *20*, 701.
- (41) Roy, A. M.; De, G. C. *J. Photochem. Photobiol., A* **2003**, *157*, 87.
- (42) Bahnemann, D. W.; Kormann, C.; Hoffmann, M. R. *J. Phys. Chem.* **1987**, *91*, 3789.
- (43) Hoffman, A. J.; Mills, G.; Yee, H.; Hoffmann, M. R. *J. Phys. Chem.* **1992**, *96*, 5546.

- (44) Bessekhoud, Y.; Chaoui, N.; Trzpit, M.; Ghazzal, N.; Robert, D.; Weber, J. V. *J. Photochem. Photobiol., A* **2006**, *183*, 218.
- (45) Chen, F.; Zhu, Y. P.; Ma, H. L.; Bo, Z. L.; Zhang, J. L. *Acta Physico-Chimica Sinica* **2004**, *20*, 1292.
- (46) Jang, J. S.; Li, W.; Oh, S. H.; Lee, J. S. *Chem. Phys. Lett.* **2006**, *425*, 278.
- (47) Tambwekar, S. V.; Venugopal, D.; Subrahmanyam, M. *Int. J. Hydrogen Energy* **1999**, *24*, 957.
- (48) Innocenti, M.; Cattarin, S.; Loglio, F.; Cecconi, T.; Seravalli, G.; Foresti, M. L. *Electrochim. Acta* **2004**, *49*, 1327.
- (49) Ueno, A.; Kakuta, N.; Park, K. H.; Finlayson, M. F.; Bard, A. J.; Campion, A.; Fox, M. A.; Webber, S. E.; White, J. M. *J. Phys. Chem.* **1985**, *89*, 3828.
- (50) Yoshimura, J.; Tanaka, A.; Kondo, J. N.; Domen, K. *Bull. Chem. Soc. Jpn.* **1995**, *68*, 2439.
- (51) Shangguan, W. F.; Yoshida, A. *Sol. Energy Mater. Sol. Cells* **2001**, *69*, 189.
- (52) Shangguan, W. F.; Yoshida, A. *J. Phys. Chem. B* **2002**, *106*, 12227.
- (53) Domen, K.; Kudo, A.; Onishi, T.; Kosugi, N.; Kuroda, H. *J. Phys. Chem.* **1986**, *90*, 292.
- (54) Kudo, A.; Tanaka, A.; Domen, K.; Maruya, K.; Aika, K.; Onishi, T. *J. Catal.* **1988**, *111*, 67.
- (55) Ewart, M.; Biaggio, I.; Zgonik, M.; Gunter, P. *Phys. Rev. B* **1994**, *49*, 5263.
- (56) Kesselman, J. M.; Weres, O.; Lewis, N. S.; Hoffmann, M. R. *J. Phys. Chem. B* **1997**, *101*, 2637.
- (57) Yariv, A.; Orlov, S. S.; Rakuljic, G. A. *J. Opt. Soc. Am., B* **1996**, *13*, 2513.

- (58) Montemezzani, G.; Gunter, P. *J. Opt. Soc. Am., B* **1990**, 7, 2323.
- (59) Park, S. W.; Huang, C. P. *J. Colloid Interface Sci.* **1987**, 117, 431.
- (60) Liu, J. C.; Huang, C. P. *Langmuir* **1992**, 8, 1851.
- (61) Duran, J. D. G.; Guindo, M. C.; Delgado, A. V.; GonzalezCaballero, F. *J. Colloid Interface Sci.* **1997**, 193, 223.
- (62) Guindo, M. C.; Zurita, L.; Duran, J. D. G.; Delgado, A. V. *Mater. Chem. Phys.* **1996**, 44, 51.
- (63) Nicolau, Y. F.; Menard, J. C. *J. Colloid Interface Sci.* **1992**, 148, 551.
- (64) Domen, K.; Kondo, J. N.; Hara, M.; Takata, T. *Bull. Chem. Soc. Jpn.* **2000**, 73, 1307.
- (65) Uchihara, T.; Matsumura, M.; Tsubomura, H. *J. Phys. Chem.* **1989**, 93, 3207.